Small-angle X-ray scattering study of the growth kinetics of CuCl nanocrystals in NaCl

R. Kranold [a*], S. Kriesen [a], M. Haselhoff [b], H.-J. Weber [b], G. Goerigk [c]

[a]*Department of Physics, Rostock University, Universitätsplatz 3, D-18051 Rostock, Germany*
[b]*Department of Physics, Dortmund University, Otto-Hahn-Straße 4, D-44221 Dortmund, Germany*
[c]*Institute of Solid State Research, Jülich Research Center, P.O. Box 1913, D-52425 Jülich, Germany*
E-mail: kranold@physik1.uni-rostock.de

The precipitation of CuCl nanocrystals in a NaCl matrix has been studied by time-resolved small-angle X-ray scattering. The experimental results suggest that the nucleation process is accelerated by lattice defects of the matrix remaining in the NaCl lattice after the dissolution of previous nanocrystals at high temperature. The evolution of structural parameters calculated from the scattering curves, such as volume fraction, mean radius and particle number density of the nanocrystals, is discussed in terms of a classical phase separation process but with specific concern for the effect of elastic strains. It was found that Ostwald ripening is effective during the whole period of observation. The effect of elastic strains results in an increase of the critical radius and a decrease of the coarsening rate. The results of the scattering experiments confirm the miscibility gap data determined by exciton spectroscopy.

Keywords: small-angle X-ray scattering; nanocrystals; phase separation

1. Introduction

The current interest in copper halide nanocrystals embedded in vitreous or crystalline matrices mainly results from two kinds of size-dependent effect, the modification of the electronic structure by quantum-confinement effects (Woggon, 1997) and the change of the phase transformation behaviour (see, *e. g.*, Onushchenko & Petrovskii, 1996). Optical absorption, in particular exciton spectroscopy, is a powerful tool for studying these phenomena. However, since positions and lineshapes of the exciton lines depend on several structural features of the nanocrystals, such as average size, size distribution, chemical composition and elastic strains, independent size-sensitive methods such as small-angle X-ray scattering (SAXS) are required to differentiate the various effects.

CuCl and NaCl form an eutectic system with an eutectic temperature $T_{eu} = 600$ K (Fig. 1). Recently, Haselhoff & Weber, (1998) were able to determine the two-solids miscibility gap on the NaCl-rich side of the phase diagram by exciton spectroscopy. The subsolidus curve, $T_s(x)$, separates the field of solid solution (SS) from the two-phase field of NaCl-rich solid solution and nearly pure CuCl crystallites (SS + CuCl). Using the model of regular solution (Christian, 1975) the experimental data were fitted by the expression

$$T_s(x) = T_c\, 2(1-2x)/\ln[(1-x)/x] \qquad (1)$$

where x is the molar fraction of CuCl. The critical temperature, T_c, was determined to be $T_c = 1580$ K.

Both crystalline structures, CuCl as well as NaCl, are cubic and the crystal axes of the CuCl nanocrystals and the NaCl matrix are parallel to each other (Fröhlich *et al.*, 1995). Thus, there is no reason that the anion sublattice collapses during the nucleation of nanocrystals. But taking into account the lattice mismatch between CuCl and NaCl (see Table 1) it is easy to imagine that the phase separation process is strongly influenced by elastic strains. Above the dissolution temperature, T_s, CuCl crystallites do not melt but they are dissolved by the diffusion of Cu^+ and Na^+ ions. In the solid solution the Cu^+ ions occupy the octahedral Na^+ sites in the NaCl lattice.

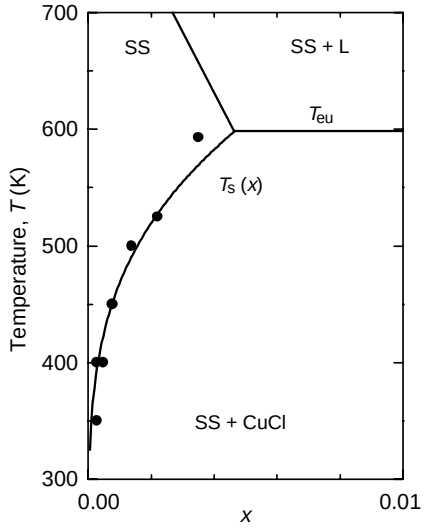

Figure 1
A section of the eutectic phase diagram NaCl-CuCl at the NaCl-rich side. T_{eu} is the eutectic temperature and x is the molar fraction of CuCl. The points represent experimentally determined dissolution temperatures, T_s. The subsolidus curve, $T_s(x)$, has been obtained by a fit of the parameter T_c in equation (1).

The aim of the present time-resolved SAXS study is a quantitative analysis of the phase separation process of CuCl-NaCl. The results are discussed in the framework of the classical theory of nucleation and growth (Christian, 1975) but with specific concern for the effect of elastic strains. Equation (1) is used and thus a verification of the results obtained by exciton spectroscopy is included, too.

2. Experimental

2.1. Sample preparation and characterization

A large single crystal of NaCl doped with CuCl (abbreviated in the following as CuCl:NaCl) was grown by the Czochralski technique. For the SAXS measurements a slab-shaped sample with a thickness of 0.6 mm was prepared by cleaving the crystal. The CuCl molar fraction of the sample, proved by wet chemical analysis, is $x = 0.002$ which corresponds to a dissolution temperature of the nanocrystals of T_s=507 K. A detailed description of the preparation method and the concentration determination is given elsewhere (Haselhoff & Weber, 1995).

A set of basic parameters for the system CuCl:NaCl used for the discussion in Section 4 is given in Table 1.

2.2. SAXS measurements

The SAXS measurements were performed with the instrument JUSIFA which is equiped with a two-dimensional position-sensitive detector (Haubold *et al.*, 1989) at DESY-HASYLAB, Hamburg. The X-ray energy used was optimized according to the sample thickness in order to maximize the scattering intensity.

 © 2003 International Union of Crystallography • Printed in Great Britain – all rights reserved

In situ growth experiments were carried out at growth temperatures of T_{gr} = 300 K, 340 K, 370 K and 400 K using a sample cell equiped with a heating unit and a gasflow cooling system. Each temperature cycle was started above the eutectic temperature with a heat treatment at T = 650 K in order to dissolve all nanocrystals which yields a reproducible state of the sample. This was checked after heating for 1 h. Then the sample was quenched to 280 K in about 20 min and again a scattering pattern was recorded. Finally the sample was heated up to the chosen growth temperature where the growth kinetics were observed over time intervals of 8 h for T_{gr} = 400 K up to 13 h for T_{gr} = 300 K. The integration time for a single scattering pattern was 10 min for T_{gr} =300 K and 5 min for the higher growth temperatures.

Table 1
Basic set of physical parameters for the system CuCl:NaCl [CuCl nanocrystals (NC) embedded in a NaCl matrix (M)].

Parameter	Reference
Eutectic temperature, T_{eu} = 600 K	(*a*)
Critical temperature in equation (1), T_c = 1580 K	(*a*)
Lattice constant of CuCl, a_0 = 0.5416 nm	(*b*)
Lattice constant of NaCl, a_0 = 0.5640 nm	(*b*)
Molar volume of CuCl, v_m(NC) = 23.92 cm^3 mol^{-1}	
Molar volume of NaCl, v_m(M) = 27.01 cm^3 mol^{-1}	
Young's modulus of CuCl, E(NC) = 13.14 GPa	(*c*)
Young's modulus of NaCl, E(M) = 43.8 GPa	(*c*)
Poisson's ratio of CuCl, γ(NC) = 0.444	(*c*)
Poisson's ratio of NaCl, γ(M) = 0.207	(*c*)
Interfacial energy between CuCl and glass, σ = 0.05 Jm^{-2}	(*d*)

References: (*a*) Haselhoff & Weber (1998); (*b*) Landolt-Börnstein (1973); (*c*) Landolt-Börnstein (1992); (*d*) Onushchenko & Petrovskii (1996).

3. Results

The measured two-dimensional scattering patterns reveal a perfect circular symmetry. In order to produce the one-dimensional scattering curves, $I(s)$, shown in Fig. 2 and Fig. 3 the scattering patterns were background corrected, radially averaged and normalized into electron scattering units (e.u.) per unit volume of the sample. The quantity s denotes the modulus of the scattering vector, $s = 4\pi \sin(\theta/2)/\lambda$, where θ is the scattering angle and λ is the X-ray wavelength.

Fig. 2 shows all scattering curves (solid lines) recorded at the different growth temperatures, T_{gr}, during the time of heat treatment, t_{gr}, together with the scattering curves obtained from the quenched state of the sample at 280 K (solid line containing the measuring points). The growth process of the nanocrystals is indicated by the evolution of the shoulders in $I(s)$ at intermediate s values, which increase in intensity and are shifted towards lower s values with increasing time t_{gr}. The scattering curves of the quenched state of the sample are somewhat different from one temperature cycle to another, without any significant trend. But it is quite obvious that processes of nucleation and growth of nanocrystals already run down during the quenching procedure.

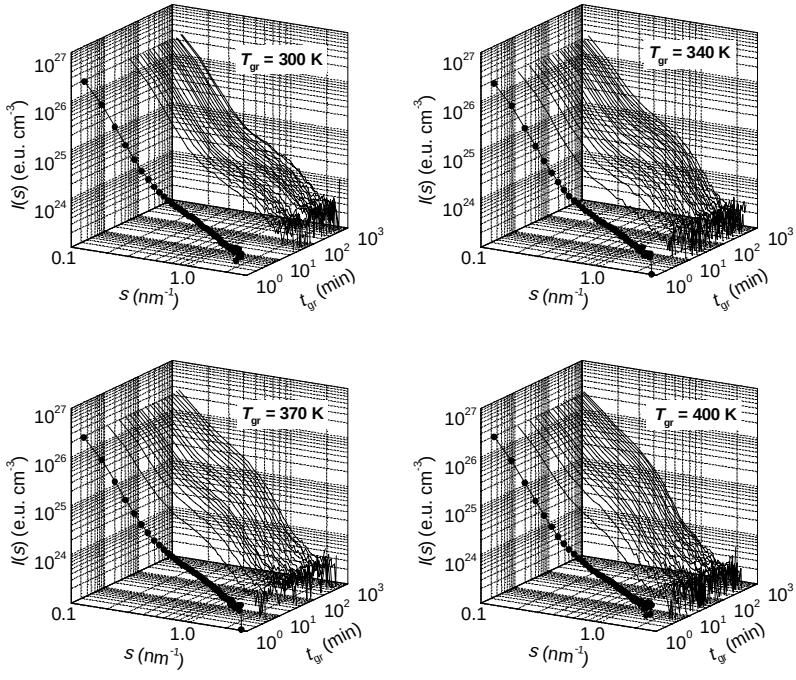

Figure 2
SAXS curves recorded *in situ* during heat treatment of one CuCl:NaCl sample at the growth temperatures, T_{gr}, given in the plots (solid lines). The scattering curves containing the measuring points were measured from the quenched state at 280 K.

The scattering of the nanocrystals is superposed by a strong power law scattering observed at the smallest s values which is in accordance with the Porod (1951) law. The heat treatment of the sample has no influence on this scattering term (see also Fig. 3).

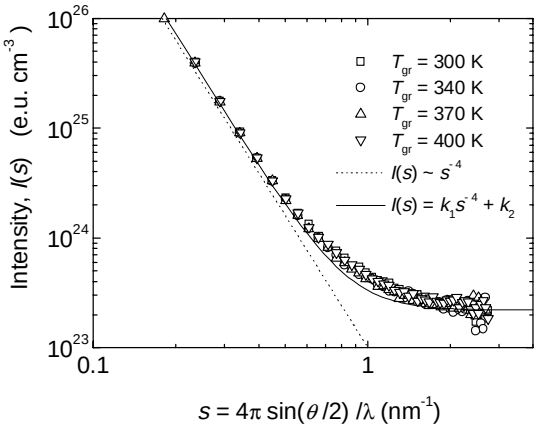

Figure 3
SAXS curves recorded *in situ* at 650 K after a heat treatment time of 1 h. The dotted line illustrates Porod's law. The $I(s)$ function given as solid line is the result of a fit.

Therefore, it can be concluded that the s^{-4} regime of $I(s)$ observed at small s values has an origin different from that of the remaining curve. In a test experiment carried out at the beamline for ultra-small-angle X-ray scattering at DESY-HASYLAB (Krosigk *et al.*, 2001), it was found that the s^{-4} scattering exists also at s values smaller than 0.04 nm^{-1}. Thus, it is estimated (Rothwell, 1970) that the scattering term $I(s) = k_1 s^{-4}$ is caused by electron density fluctuations larger than 175 nm in size. Probably, the s^{-4} scattering at small s values is the Porod tail of the scattering curve produced by very large surface heterogeneities of the sample. In any case, it has to be eliminated before any more detailed analysis of $I(s)$.

In Fig. 3 scattering curves are shown obtained at the outset of each temperature cycle after a heat treatment of the sample at 650 K for 1 h. Evidently, using this heat treatment a defined state of the sample is reproduced completely. The main features of the intensity function are the power low scattering, $I(s) = k_1 s^{-4}$, at small s values discussed above and a s-independent scattering term, k_2, observed at large s values. The term k_2 can be attributed to the scattering of Cu^+ ions and other point defects randomly distributed in the sample (Guinier & Fournet, 1955).

There is no indication for non-dissolved nanocrystals in the scattering curves. However, the result of a least-squares fit of the expression $I(s) = k_1 s^{-4} + k_2$ to the scattering data, displayed by the solid line in Fig. 3, reveals a residual intensity arising from very small inhomogeneities in the sample whose nature is unknown at this point. It can be imagined that the NaCl lattice is not yet completely restored after the dissolution of the nanocrystals. Remaining "scars" might produce the weak scattering effect observed, though they should influence the primary nucleation of seeds drastically.

Structural parameters of the nanocrystals were extracted from the scattering curves shown in Fig. 2 after subtraction of the averaged SAXS intensities obtained from the state of the sample where all nanocrystals are dissolved (Fig. 3). For this the nanocrystals (NC) were considered to be spherical particles with the uniform electron density of bulk CuCl but varying radii, R, embedded in a uniform matrix (M) of pure NaCl. So, the scattering intensity of the nanocrystals can be expressed by:

$$I(s) = \int_0^\infty N(R)\left[f(s,R,\Delta\rho)\right]^2 \mathrm{d}R \qquad (2)$$

where $N(R)$ is the radius distribution function and

$$f(s,R,\Delta\rho) = \Delta\rho 4\pi R^3\left[\sin(sR) - sR\cos(sR)\right]/(sR)^3 \qquad (3)$$

is the scattering amplitude (Guinier & Fournet, 1955) with $\Delta\rho = \rho_{NC} - \rho_M$ being the difference in electron density calculated from the data given in Table 1. Using a single log-normal size distribution (LND),

$$N(R) = N_v \exp\left[-(\ln R - \ln R_0)^2 / 2\ln^2\sigma_g\right] \quad , \qquad (4)$$

expression (2) was found to be well suited to approximate the experimental data; N_v = particle number density of the nanocrystals, R_0 = geometric mean and σ_g = geometric standard deviation of the distribution are free parameters. In Fig. 4 the LND function resulting from a fit of equations (2), (3) and (4) to the experimental scattering curve of a CuCl:NaCl sample is shown together with the size distribution of the nanocrystals calculated by the Fourier transform technique (FTT) described by Walter *et al.* (1985), which does not require any *a priori* assumption about the form of the distribution function.

Additionally to the number density, N_v, of the nanocrystals obtained as a fit parameter, the mean radius of the size distribution,

$$\langle R\rangle = \int_0^\infty R N(R)\,\mathrm{d}R \quad , \qquad (5)$$

and the volume fraction of the nanocrystals,

$$w = (4/3)\pi\int_0^\infty R^3 N(R)\,\mathrm{d}R \quad , \qquad (6)$$

were calculated from each LND function. The results are summarized in Fig. 5.

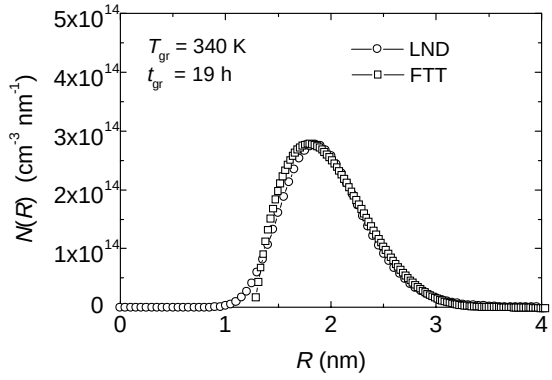

Figure 4
Size distribution, $N(R)$, of CuCl nanocrystals in NaCl grown at 340 K during 19 h. The log-normal distribution (LND) is the result of a fit of equations (2), (3) and (4) to the experimental SAXS curve. The distribution denoted by FTT was calculated using a Fourier transform technique (Walter *et al.*, 1985) without *a priori* assumptions concerning the form of the distribution function.

4. Discussion

It has been mentioned above that the crystal axis of CuCl nanocrystals and that of the NaCl matrix are be parallel to each other (Fröhlich *et al.*, 1995). The shape of the nanocrystals has rarely been studied. Recently, it has been suggested that the nanocrystal shape

ranges from cubic to spherical (Sakakura & Masumoto, 1997). As the measured two-dimensional SAXS patterns reveal perfect circular symmetry, for the determination of the structural parameters shown in Fig. 5, spherical nanocrystals were assumed. But it is worth mentioning that values of the volume fraction, *w*, calculated from the integrated intensity (Porod, 1951), *i.e.* without the assumption of a spherical shape of the nanocrystals, are only marginally varying from those shown in Fig. 5 (Kriesen, 2000).

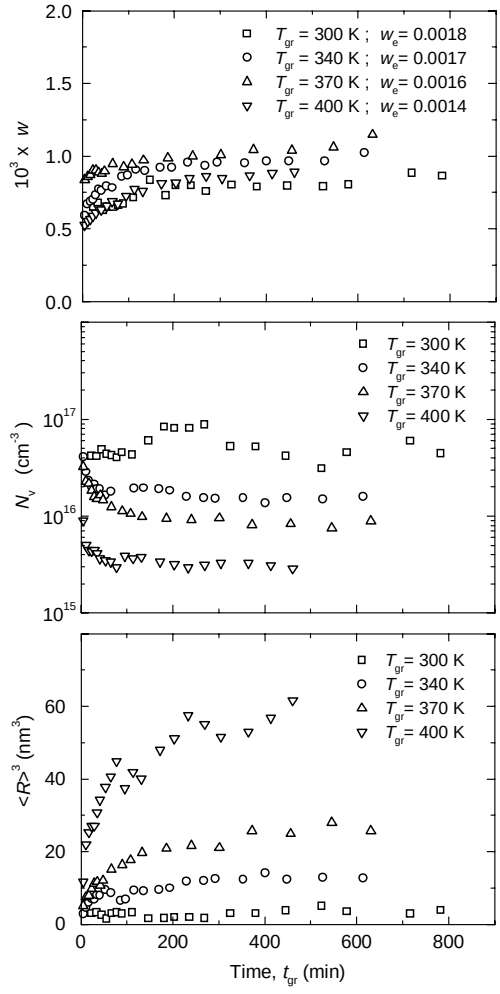

Figure 5
Time dependence of the volume fraction, the particle number density and the cube of the mean radius of CuCl nanocrystals grown in NaCl at the growth temperatures, T_{gr}, given in the plots. The equilibrium values of the volume fraction, w_e, were calculated from equation (7).

The equilibrium solubility, x_s, of Cu^+ ions in NaCl at the different growth temperatures, T_{gr}, is obtained from equation (1). So, the equilibrium value of the volume fraction, w_e, of CuCl nanocrystals in a NaCl matrix can be calculated by the lever rule:

$$w_e = (x_0 - x_s)\,v_m(\mathrm{NC})/[(x_{NC} - x_s)\,v_m(\mathrm{M})] \qquad (7)$$

where v_m(NC) and v_m(M) are the molar volumes of CuCl and NaCl, respectively. The molar fraction of CuCl in the nanocrystals was assumed to be $x_{NC} = 1$. The calculated w_e values are given in the upper plot of Fig. 5.

In the classical theory (Christian, 1975), phase separation processes are considered in three different stages: (i) nucleation of seeds, (ii) independent growth of seeds to clusters and (iii) competitive cluster growth where the large clusters grow at the expense of the smaller ones. The latter stage is called coarsening or Ostwald ripening. From the evolution of N_v shown in Fig. 5, that (apart from a short time interval in the beginning of the heat treatment at 300 K) decreases with time, it can be concluded that Ostwald ripening is effective during the whole period of observation. With other words, the earlier stages of the phase separation process could not be directly observed. The scattering curves measured from the quenched state of the sample (Fig. 2) evidently reveal the presence of small nanocrystals. Thus, the processes of nucleation and growth run down unexpected fast. One reason for these findings may be that the NaCl lattice remains disturbed after the dissolution of the nanocrystals at 650 K as suggested by the scattering curves shown in Fig. 3. This presumption is supported by the observation of local assemblies of Schottky defects related to big nanocrystals in a scanning near-field optical microscope (Diegeler *et al.*, 1998). No matter how, it must be assumed that in the beginning of the heat treatment at the different growth temperatures the sample contains a certain number of athermal nuclei.

The evolution of the structural parameters shown in Fig. 5 gives evidence that for non of the different growth temperatures the sample is in the asymptotic stage of Ostwald ripening described by the classical LSW theory (Lifshitz & Slyozov, 1961; Wagner, 1961). The equilibrium volume fraction, w_e, of the nanocrystalline phase has not yet precipitated, but w increases with time. Thus, N_v decreases more slowly than expected for the asymptotic stage (Ardell, 1997). Furthermore, the shape of the size distribution of the nanocrystals (Fig. 4, FTT), even obtained from later time stages, is different from that predicted by the LSW theory. It should be noted that for the CuCl:NaCl sample the assumption of vanishing volume fractions made in the LSW theory is well fulfilled.

On the other hand, it has been found (Möller *et al.*, 1995 and references there in) that the growth law $\langle R(t)\rangle^3 = \langle R(0)\rangle^3 + const.\ t$, predicted for diffusion controlled Ostwald ripening by the LSW theory, frequently can be observed already in the non-asymptotic stage, even for particle systems with relatively large volume fractions. However, a plot of $\langle R\rangle^3$ *versus* t (at the bottom of Fig. 5) shows that the coarsening rate of the CuCl nanocrystals decreases with increasing time, t_{gr}. This behaviour can be explained by the elastic reaction of the matrix which is of particular significance if, as in the present case, the mobility of the segregating species is much higher than that of the building units of the matrix (Möller *et al.*, 1996).

For the first non-asymptotic stage of Ostwald ripening in dilute systems the volume fraction of precipitates is related to their current mean radius, $\langle R\rangle$, by

$$w = w_e - w_e\, R^* / \langle R \rangle \qquad (8)$$

(Schmelzer, 1990; Ardell, 1997) where R^* can be understood as the critical Gibbs-Thomson radius, R_c. For the CuCl nanocrystals R_c can be calculated (Christian, 1975) by

$$R_c = 2\sigma\, v_m(\mathrm{NC})/\Delta\mu \qquad (9)$$

where σ is the interfacial energy and Δμ is the thermodynamic driving force of the phase separation process. For the case of a regular solution (Christian, 1975) holds:

$$\Delta\mu(x,T) = \mathrm{N_A k_B} T \ln(x/x_s) + 2\mathrm{N_A k_B} T_c\left[(1-x)^2 - (1-x_s)^2\right] \qquad (10)$$

with N_A = Avogadro's number; k_B = Boltzmann's constant.

Elastic strains resulting from the lattice mismatch, δ, between the CuCl nanocrystals (NC) and the NaCl matrix (M) increases the critical radius (Schmelzer & Gutzow, 1988):

$$R_c = 2\sigma\, v_m(\mathrm{NC})/[\Delta\mu - \varepsilon\, v_m(\mathrm{NC})] \qquad (11)$$

with $$\varepsilon = \frac{E_{NC}\, E_M}{3[2\, E_M (1-2\gamma_{NC}) + E_{NC}(1+\gamma_M)]}\delta^2$$

and $$\delta = [\nu_m(M) - \nu_m(NC)] / \nu_m(NC)$$

where E stands for Young's modulus and γ for Poisson's ratio. The values of the critical radius calculated from equations (9) and (11), respectively, are given in Table 2.

Table 2
Critical radii of CuCl nanocrystals in CuCl:NaCl.

T_{gr} (K)	R^* (nm) equation (8)	R_c (nm) equation (9)	R_c (nm) equation (11)
300	0.8	0.23	0.31
340	1.0	0.28	0.43
370	1.1	0.34	0.58
400	1.6	0.44	0.95

In Fig. 6 the volume fraction of the nanocrystals is plotted *versus* their reciprocal mean radius. The solid lines in Fig. 6 illustrate that equation (8) matches to the experimental data. The R^* values obtained, corresponding to $w = 0$, are also given in Table 2. Considering the uncertainty of the experimental SAXS data and in particular that of the only available value for the interfacial energy, σ, a satisfactory agreement of the SAXS parameters R^* with the calculated R_c values is obtained. It should be noted that there is evidence that σ is larger in CuCl:NaCl than in a vitreous matrix (Haselhoff *et al*., 1999).

Furthermore, in a first order approximation the reciprocal values of the critical radii linearly depend on temperature according to

$$1/R_c = const.(T_s - T_{gr}) \quad . \qquad (12)$$

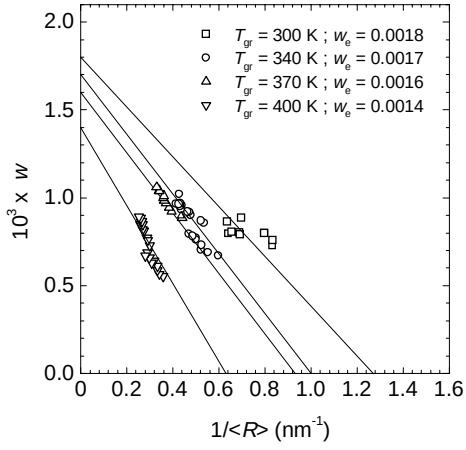

Figure 6
Volume fraction of CuCl nanocrystals in NaCl *versus* their reciprocal mean radius. The corresponding growth temperatures, T_{gr}, and the equilibrium volume fractions, w_e, are given in the plot. The solid lines illustrate that equation (8) matches the experimental data.

The SAXS results obey equation (12) very well and their extrapolation yields T_s = 500 K, which is in good agreement with T_s = 507 K calculated from equation (1). So, it can be stated that the set of SAXS data obtained in this study is completely consistent with the miscibility gap data (equation (1) with T_c = 1580 K) determined by optical absorption experiments.

5. Conclusions

The results of the present time-resolved SAXS study of the precipitation of CuCl nanocrystals in a NaCl matrix suggest that the phase separation process is strongly influenced by lattice defects of the matrix and by elastic strains. The effect of elastic strains produced by the lattice mismatch between matrix and nanocrystals results in an increase of the critical radius. In the Ostwald ripening of the nanocrystals, elastic strains cause a retardation of the coarsening process.

The SAXS results confirm the parameter T_c of the miscibility gap previously determined by exciton spectroscopy. The size distributions, $N(R)$, of the nanocrystals calculated in the course of the present SAXS study are useful to improve the analysis of the measured exciton spectra as will be shown in a forthcoming paper.

This work was financially supported by the Deutsche Forschungsgemeinschaft.

References

Ardell, A. J. (1997). *Mater. Sci. Eng.* A, **238**, 108-120.
Christian, J. W. (1975). *The Theory of Transformations in Metals and Alloys*, 2nd edition, Oxford: Pergamon Press.
Diegeler, A., Haselhoff, M., Rammensee, W. & Weber, H.-J. (1998). *Solid State Commun.* **105**, 269-272.
Fröhlich, D., Haselhoff, M. & Reimann, K. (1995*). Solid State Commun.* **94**, 189-191.
Guinier, A. & Fournet, G. (1955). *Small-Angle Scattering of X-rays*, New York: Wiley.
Haselhoff. M. & Weber, H.-J. (1995). *Mat. Res. Bull.* **30**, 607-612.
Haselhoff, M. & Weber, H.-J. (1998). *Phys. Rev.* B, **58**, 5052-5061.
Haselhoff, M., Reimann, K. & Weber, H.-J. (1999). *Eur. Phys. J.* B, **12**, 147-155.
Haubold, H. G., Gruenhagen, K., Wagner, M., Jungbluth, H., Heer, H., Pfeil, A., Rongen, H., Brandenburg, G., Moeller, R., Matzerath, J., Hiller, P. & Halling, H. (1989). *Rev. Sci. Instrum.* **60**, 1943-1946.
Kriesen, S. (2000). Diploma thesis, Rostock University, Germany.
Krosigk, von, G., Cunis, S., Gehrke, R. & Kranold, R. (2001). *Nucl. Instrum. Meth. Phys. Res.* A, **467-468**, 1088-1091.
Landolt-Börnstein (1973). *Zahlenwerte und Funktionen aus Naturwissenschaft und Technik*, Neue Serie, Band **III/7**, Berlin: Springer.
Landolt-Börnstein (1992). *Zahlenwerte und Funktionen aus Naturwissenschaft und Technik*, Neue Serie, Band **III/29a**, Berlin: Springer.
Lifshitz, I. M. & Slyozov, V. V. (1961). *J. Phys. Chem. Solids*, **19**, 35-50.
Möller, J., Kranold, R., Schmelzer, J. & Lembke, U. (1995). *J. Appl. Cryst.* **28**, 553-560.
Möller, J., Schmelzer, J. & Avramov, I. (1996). *Phys. Status Solidi* B, **196**, 49-62.
Onushchenko, A. A. & Petrovskii, G. T. (1996). *J. Non-Cryst. Solids*, **196**, 73-78.
Porod, G. (1951). *Kolloid. Z.* **124**, 83-113.
Rothwell, W. S. (1970*). J. Appl. Phys.* **41**, 4459-4461.
Sakakura, N. & Masumoto, Y. (1997). *Phys. Rev.* B, **56**, 4051-4055.
Schmelzer, J. & Gutzow, I. (1988). *Z. phys. Chem.* **269**, 753-767.
Schmelzer, J. (1990). *Phys. Status Solidi* B, **161**, 173-177.
Wagner, C. (1961). *Z. Elektrochem.* **65**, 581-591.
Walter, G., Kranold, R., Gerber, T., Baldrian, J. & Steinhart, M. (1985). *J. Appl. Cryst.* **18**, 205-213.
Woggon, U. (1997). *Optical Properties of Semiconductor Quantum Dots, Springer Tracts in Modern Physics* **136,** Berlin: Springer.